Superbroadband near-infrared emission and energy transfer in Pr^{3+}-Er^{3+} codoped fluorotellurite glasses

Bo Zhou,[1,4] Lili Tao,[2] Yuen H. Tsang,[2,5] Wei Jin,[1,6] and Edwin Yue-Bun Pun[3]

[1]*Department of Electrical Engineering, The Hong Kong Polytechnic University, Kowloon, Hong Kong, China*
[2]*Department of Applied Physics, The Hong Kong Polytechnic University, Kowloon, Hong Kong, China*
[3]*Department of Electronic Engineering, City University of Hong Kong, Kowloon, Hong Kong, China*
[4]*eebzhou@polyu.edu.hk*
[5]*yuen.tsang@polyu.edu.hk*
[6]*eewjin@polyu.edu.hk*

Abstract: We report the first demonstration of superbroadband emission extending from 1.30 to 1.68 μm in praseodymium(Pr^{3+})-erbium(Er^{3+}) codoped fluorotellurite glasses under 488 nm excitation. This superbroad near-infrared emission is contributed by the Pr^{3+}: $^1D_2 \rightarrow {}^1G_4$ and Er^{3+}: $^4I_{13/2} \rightarrow {}^4I_{15/2}$ transitions which lead to emissions located at 1.48 and 1.53 μm, respectively. The quenching of the Pr^{3+} emission resulted from the cross relaxation $[^1D_2, {}^3H_4] \rightarrow [^1G_4, {}^3F_{3,4}]$ was effectively compensated by the codoping of Er^{3+}. The results suggest that, other than the heavy-metal and transition-metal elements of active bismuth (Bi), nickel (Ni), chromium (Cr), etc., Pr^{3+}-Er^{3+} codoped system is a promising alternative for the broadband near-infrared emission covering the expanded low-loss window.

OCIS codes: (160.5690) Rare-earth-doped materials; (300.6280) Spectroscopy, fluorescence and luminescence; (230.2285) Fiber devices and optical amplifiers.

References and links

1. G. A. Thomas, B. I. Shraiman, P. F. Glodis, and M. J. Stephen, "Towards the clarity limit in optical fibre," Nature **404**(6775), 262–264 (2000).
2. S. Kasap, "Optoelectronics" in *The Optics Encyclopedia* edited by T. Brown, K. Creath, H. Kogelnik, M. A. Kriss, J. Schmit, and M. J. Weber (Wiley-VCH, 2004), vol. 4, pp. 2237–2284.
3. K. Murata, Y. Fujimoto, T. Kanabe, H. Fujita, and M. Nakatsuka, "Bi-doped SiO_2 as a new laser material for an intense laser," Fusion Eng. Des. **44**(1–4), 437–439 (1999).
4. M. Peng, J. Qiu, D. Chen, X. Meng, and C. Zhu, "Superbroadband 1310 nm emission from bismuth and tantalum codoped germanium oxide glasses," Opt. Lett. **30**(18), 2433–2435 (2005).
5. I. A. Bufetov and E. M. Dianov, "Bi-doped fiber lasers," Laser Phys. Lett. **6**(7), 487–504 (2009).
6. V. G. Truong, L. Bigot, A. Lerouge, M. Douay, and I. Razdobreev, "Study of thermal stability and luminescence quenching properties of bismuth-doped silicate glasses for fiber laser applications," Appl. Phys. Lett. **92**(4), 041908 (2008).
7. M. Y. Sharonov, A. B. Bykov, V. Petricevic, and R. R. Alfano, "Spectroscopic study of optical centers formed in Bi-, Pb-, Sb-, Sn-, Te-, and In-doped germanate glasses," Opt. Lett. **33**(18), 2131–2133 (2008).
8. T. Suzuki, G. S. Murugan, and Y. Ohishi, "Optical properties of transparent Li_2O-Ga_2O_3-SiO_2 glass-ceramics embedding Ni-doped nanocrystals," Appl. Phys. Lett. **86**(13), 131903 (2005).
9. Y. C. Huang, Y. K. Lu, J. C. Chen, Y. C. Hsu, Y. M. Huang, S. L. Huang, and W. H. Cheng, "Broadband emission from Cr-doped fibers fabricated by drawing tower," Opt. Express **14**(19), 8492–8497 (2006).
10. M. Peng, G. Dong, L. Wondraczek, L. Zhang, N. Zhang, and J. Qiu, "Discussion on the origin of NIR emission from Bi-doped materials," J. Non-Cryst. Solids **357**(11–13), 2241–2245 (2011).
11. See, for example, *Rare-Earth-Doped Fiber Lasers and Amplifiers* (Second Edition, Revised and Expanded) edited by M. J. F. Digonnet (Marcel Dekker, 2009), and references therein.
12. B. Zhou, H. Lin, and E. Y. B. Pun, "Tm^{3+}-doped tellurite glasses for fiber amplifiers in broadband optical communication at 1.20 μm wavelength region," Opt. Express **18**(18), 18805–18810 (2010).
13. B. Zhou, H. Lin, B. J. Chen, and E. Y. B. Pun, "Superbroadband near-infrared emission in Tm-Bi codoped sodium-germanium-gallate glasses," Opt. Express **19**(7), 6514–6523 (2011).
14. D. R. Simons, A. J. Faber, and H. de Waal, "Pr^{3+}-doped GeS_x-based glasses for fiber amplifiers at 1.3 μm," Opt. Lett. **20**(5), 468–470 (1995).

#159575 - $15.00 USD Received 9 Dec 2011; revised 23 Mar 2012; accepted 29 Mar 2012; published 14 May 2012

15. Y. G. Choi, K. H. Kim, B. J. Park, and J. Heo, "1.6 μm emission from Pr^{3+}: ($^3F_3$, $^3F_4$)→$^3H_4$ transition in Pr^{3+}- and Pr^{3+}/Er^{3+}-doped selenide glasses," Appl. Phys. Lett. **78**(19), 1249–1251 (2001).
16. B. Zhou and E. Y. B. Pun, "Superbroadband near-IR emission from praseodymium-doped bismuth gallate glasses," Opt. Lett. **36**(15), 2958–2960 (2011).
17. J. Dong, Y. Q. Wei, A. Wonfor, R. V. Penty, I. H. White, J. Lousteau, G. Jose, and A. Jha, "Dual-pumped tellurite fiber amplifier and tunable laser using Er/Ce codoping scheme," IEEE Photon. Technol. Lett. **23**(11), 736–738 (2011).
18. B. R. Judd, "Optical absorption intensities of rare-earth ions," Phys. Rev. **127**(3), 750–761 (1962).
19. G. S. Ofelt, "Intensities of crystal spectra of rare-earth ions," J. Chem. Phys. **37**(3), 511–520 (1962).
20. R. T. Génova, I. R. Martin, U. R. Rodriguez-Mendoza, F. Lahoz, A. D. Lozano-Gorrin, P. Nunez, J. Gonzalez-Platas, and V. Lavin, "Optical intensities of Pr^{3+} ions in transparent oxyfluoride glass and glass-ceramic. Applications of the standard and modified Judd-Ofelt theories," J. Alloy. Comp. **380**(1–2), 167–172 (2004).
21. L. R. Moorthy, M. Jayasimhadri, A. Radhapathy, and R. V. S. S. N. Ravikumar, "Lasing properties of Pr^{3+}-doped tellurofluorophosphate glasses," Mater. Chem. Phys. **93**(2–3), 455–460 (2005).
22. V. Nazabal, S. Todoroki, A. Nukui, T. Matsumoto, S. Suehara, T. Hondo, T. Araki, S. Inoue, C. Rivero, and T. Cardinal, "Oxyfluoride tellurite glasses doped by erbium: thermal analysis, structural organization and spectral properties," J. Non-Cryst. Solids **325**(1–3), 85–102 (2003).
23. S. Dai, J. Zhang, C. Yu, G. Zhou, G. Wang, and L. Hu, "Effect of hydroxyl groups on nonradiative decay of Er^{3+}: $^4I_{13/2}$→$^4I_{15/2}$ transition in zinc tellurite glasses," Mater. Lett. **59**(18), 2333–2336 (2005).
24. P. S. Golding, S. D. Jackson, T. A. King, and M. Pollnau, "Energy transfer processes in Er^{3+}-doped and Er^{3+}, Pr^{3+}-codoped ZBLAN glasses," Phys. Rev. B **62**(2), 856–864 (2000).
25. S. H. Park, D. C. Lee, J. Heo, and D. W. Shin, "Energy transfer between Er^{3+} and Pr^{3+} in chalcogenide glasses for dual-wavelength fiber-optic amplifiers," J. Appl. Phys. **91**(11), 9072–9077 (2002).
26. Y. Ohishi, T. Kanamori, J. Temmyo, M. Wada, M. Yamada, M. Shimizu, K. Yoshino, H. Hanafusa, M. Horiguchi, and S. Takahashi, "Laser diode pumped Pr^{3+}-doped and Pr^{3+}-Yb^{3+}-codoped fluoride fiber amplifiers operating at 1.3 μm," Electron. Lett. **27**(22), 1995–1996 (1991).
27. X. Zhu and R. Jain, "Watt-level Er-doped and Er-Pr-codoped ZBLAN fiber amplifiers at the 2.7-2.8 microm wavelength range," Opt. Lett. **33**(14), 1578–1580 (2008).
28. T. Schweizer, D. W. Hewak, B. N. Samson, and D. N. Payne, "Spectroscopic data of the 1.8-, 2.9-, and 4.3-μm transitions in dysprosium-doped gallium lanthanum sulfide glass," Opt. Lett. **21**(19), 1594–1596 (1996).
29. D. Yang, E. Y. B. Pun, B. Chen, and H. Lin, "Radiative transitions and optical gains in Er^{3+}/Yb^{3+} codoped acid-resistant ion exchanged germanate glass channel waveguides," J. Opt. Soc. Am. B **26**(2), 357–363 (2009).
30. A. Jha, S. Shen, and M. Naftaly, "Structural origin of spectral broadening of 1.5-μm emission in Er^{3+}-doped tellurite glass," Phys. Rev. B **62**(10), 6215–6227 (2000).

1. Introduction

Development of superbroadband near-infrared luminescence sources for broadband optical amplifiers and tunable lasers covering entirely the expanded low-loss telecommunication window (~1.2-1.7 μm) attracts considerable attention, in particular, after the progress made in the production of hydroxyl (OH^-)-free silica fibers (dry optical fibers) [1,2]. Previous investigations were focused on the bismuth (Bi) [3–6], and then an extension to other heavy metal (HM) and transition metal (TM) ions, such as nickel (Ni), chromium (Cr), lead (Pb), etc. [7–9]. However, the bandwidth and peak wavelength of the broadband emissions from HM/TM ions depend sensitively on the host matrix and the excitation wavelength, and also the luminescence origin for some of them requires further studies [10]. To date, there has been little work reports on the superbroadband luminescence from rare earth (RE) doped systems, although they play crucial roles as optical amplifiers and laser sources in telecommunication systems [11]. Typical RE emissions/amplifications cover only separate C-, L-, S-, E-, and O-bands. Thus, novel host matrix, dual-pump configurations, nanostructures, and REs codoping schemes have been investigated to further improve the bandwidth and the quantum efficiency [11]. Recently, broadband emissions located at 1.20 and 1.47 μm were observed in thulium (Tm^{3+})-doped glasses [12,13], and a broader emission band from 1.0 to 1.7 μm was obtained using Tm-Bi codoping scheme by taking advantage of the Bi 1.3 μm emission [13].

Praseodymium (Pr^{3+}) shows promising to achieve some novel near-infrared emissions due to the rich multiple energy levels. Apart from the well-known 1.3 μm emission ($^1G_4$→$^3H_5$ transition) [14], an emission around 1.6 μm from the $^3F_{3,4}$→$^3H_4$ transition was also observed in Pr^{3+}-doped selenide glass [15]. We recently observed superbroadband near-infrared luminescence in Pr^{3+}-doped bismuth gallate glass [16]. However, the low transmission of bismuth gallate glass in the blue region resulted in a depression of the pump efficiency using blue light, at which Pr^{3+} possesses intense absorption bands. In addition, the Pr^{3+} near-infrared

#159575 - $15.00 USD Received 9 Dec 2011; revised 23 Mar 2012; accepted 29 Mar 2012; published 14 May 2012

emission, especially at the longer wavelength side, was seriously quenched by the cross relaxation [$^1D_2$, $^3H_4$]→[$^1G_4$, $^3F_{3,4}$] because of the intense ground-state absorption $^3F_{3,4}$←$^3H_4$ which is overlapped with the Pr^{3+} emission.

In the present work, we propose Pr^{3+}-Er^{3+} codoping scheme to achieve the superbroadband near-infrared emission for the first time to our best knowledge. Efficient Er^{3+} 1.53 μm emissions/amplifications have already been demonstrated under 488 nm excitation (into the absorption band Er^{3+}: $^4F_{7/2}$←$^4I_{15/2}$) [11]. Fluorotellurite glasses were selected as host because of their broad transmission window, good mechanical properties and chemical durability, and optical amplification and laser operation have been achieved in tellurite glass fibers [17].

2. Experimental

Glass samples were prepared by melting well-mixed high purity materials of lanthanum fluoride (LaF_3), barium fluoride (BaF_2), barium carbonate ($BaCO_3$), zinc oxide (ZnO), and tellurium oxide (TeO_2) following a standard melt-quenching procedure as described in [12]. Praseodymium fluoride (PrF_3) and erbium fluoride (ErF_3) were used as RE dopants with doping levels of $x$$PrF_3$-$y$$ErF_3$ mol% where x = 0, 0.1, 0.2, 0.3; y = 0.1, and x = 0.3; y = 0, 0.05. LaF_3 and BaF_3 were added to modify the ligand field between the RE sites and the matrix. The as-prepared glasses were cut and optically polished for optical measurements.

The refractive index of the glass samples was measured using a Metricon 2010 prism coupler. The Raman spectrum of undoped glass sample was measured using a HORIBA Jobin Yvon HR800 Raman spectrometer with a 488 nm laser excitation source. The absorption spectra were recorded using a Perkin Elmer UV-VIS-NIR Lambda 19 double beam spectrophotometer. The visible and infrared emission spectra were recorded using an Edinburgh Instruments FLSP920 spectrofluorometer. The wavelengths of excitation sources were tuned from a continuous xenon lamp by a monochromator. The excitation spectra were recorded using the same setup with a continuous wavelength xenon lamp as the excitation source. The emission decay curves were recorded using the same setup with a flash xenon lamp as the excitation source. All the measurements were carried out at room temperature.

3. Results and discussion

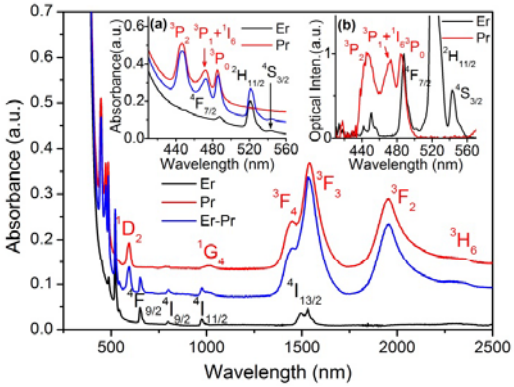

Fig. 1. Absorption spectra of (0.3 mol%)Pr^{3+}-doped, (0.1 mol%)Er^{3+}-doped, and (0.3mol%)Pr^{3+}-(0.1mol%)Er^{3+} codoped fluorotellurite glasses. Inset (a) shows the details of absorption spectra in wavelength region 410-560 nm; Inset (b) shows the excitation spectra monitored at 1.42 and 1.53 μm wavelengths from Pr^{3+}- and Er^{3+}-singly doped samples, respectively.

Figure 1 shows the absorption spectra of Pr^{3+}-, Er^{3+}-singly doped and Pr^{3+}-Er^{3+} codoped samples. All the absorption bands observed are due to the electronic transitions from the ground-state to the respective excited states as indicated in Fig. 1. The transparency at the blue wavelength region is much higher than bismuth gallate glass, which would allow efficient pumping with blue light sources. It is interesting to observe that both Pr^{3+} and Er^{3+} possess absorptions around 488 nm [see inset (a) of Fig. 1]; they correspond to the Pr^{3+}:

#159575 - $15.00 USD Received 9 Dec 2011; revised 23 Mar 2012; accepted 29 Mar 2012; published 14 May 2012

$^3P_0 \leftarrow {}^3H_4$ and Er^{3+}: $^4F_{7/2} \leftarrow {}^4I_{15/2}$ transitions, respectively. This resonant energy-level matching makes it possible to achieve the superbroadband emission in the Pr^{3+}-Er^{3+} codoping scheme by pumping with a single-wavelength light source. This is in agreement with the excitation spectra, as shown in inset (b) of Fig. 1.

Table 1. Spontaneous transition parameters of Pr^{3+} and Er^{3+} in fluorotellurite glass

Transition	Energy (cm^{-1})	Spontaneous transition probability (s^{-1})	Branch ratio (%)	Radiative lifetime (ms)
Pr^{3+}: $^1D_2 \rightarrow {}^1G_4$	7013	880.1	11.1	0.126
Er^{3+}: $^4I_{13/2} \rightarrow {}^4I_{15/2}$	6527	454.1[a]	100	2.202

[a]The magnetic dipole transition contribution is 77.4 s^{-1}.

Using the absorption spectra, Judd-Ofelt analysis was performed [18,19]. The values of intensity parameters Ω_t (t = 2, 4, 6) are calculated to be (3.57, 6.60, 5.18) × 10^{-20} cm^2, and (5.62, 1.12, 1.78) × 10^{-20} cm^2 for Pr^{3+}- and Er^{3+}-singly doped samples, respectively, using a least-squares fitting of the experimental and theoretical electric dipole oscillator strengths. The larger Ω_2 value of Pr^{3+} in fluorotellurite than those other fluoride contained oxide glasses indicates a stronger asymmetry and covalent environment of Pr^{3+} in fluorotellurite glass [20,21]. A similar result is also obtained for Er^{3+}-doping, in which the value of Ω_2 is larger than those ZnF_2 contained tellurite glasses [22]. The spontaneous transition properties of Pr^{3+} and Er^{3+} are listed in Table 1. The spontaneous transition probability of Pr^{3+}: $^1D_2 \rightarrow {}^1G_4$ is 880.1 s^{-1} (with branch ratio of 11.1%), which is comparable to that of Pr^{3+} in bismuth gallate glass [16]. Regarding the Er^{3+}: $^4I_{13/2} \rightarrow {}^4I_{15/2}$, the spontaneous transition probability (454.1 s^{-1}) is larger than that in ZnF_2 contained and oxide-based tellurite glasses [22,23].

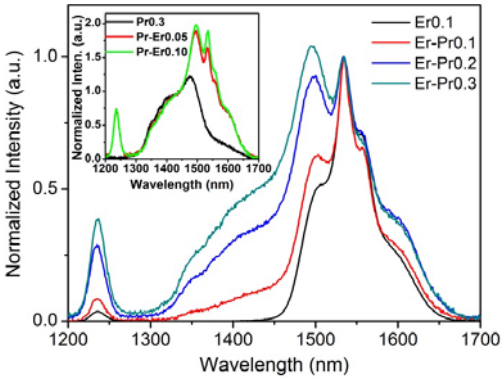

Fig. 2. Normalized near-infrared emission spectra of Er^{3+}-doped and Pr^{3+}-Er^{3+} codoped samples with respect to the Er^{3+} 1.53 μm emission. Inset shows the normalized emission spectra with respect to the Pr^{3+} emission at 1.42 μm wavelength. The excitation wavelength is 488 nm.

Figure 2 compares the near-infrared emissions of Pr^{3+}-Er^{3+} codoped samples under 488 nm excitation for different Pr^{3+} concentrations. Compared with the narrower Er^{3+} 1.53 μm emission band (Er^{3+}: $^4I_{13/2} \rightarrow {}^4I_{15/2}$ transition), the emission in Pr^{3+}-Er^{3+} codoped samples shows an obvious extension and enhancement in the short wavelength side, resulting in a superbroad emission band at 1.3-1.68 μm range. The broad emission at short wavelength region is contributed by the Pr^{3+}: $^1D_2 \rightarrow {}^1G_4$ transition, which leads to a broad near-infrared emission band under blue excitation. This is in agreement with the Pr^{3+}-doped bismuth gallate glass [16]. Figure 2 inset shows the normalized emissions of the Pr^{3+}-Er^{3+} codoped samples with different Er^{3+} concentrations. The composite near-infrared emission at the longer wavelength side is enhanced by incorporation of Er^{3+}. The emission observed at 1.23 μm is due to the Er^{3+}: $^4S_{3/2} \rightarrow {}^4I_{11/2}$ transition, which shows a relative increasing trend with the increase of Pr^{3+}.

Figure 3(a) shows the decay curves of Pr^{3+}: $^1D_2$ measured at a monitoring wavelength of 1.42 μm. This wavelength is significantly away from the Er^{3+} 1.53 μm emission band, and

#159575 - $15.00 USD Received 9 Dec 2011; revised 23 Mar 2012; accepted 29 Mar 2012; published 14 May 2012

hence the effect of the Er^{3+} 1.53 μm emission on the decay measurement can be ignored. Since the decay curves recorded deviate slightly from the single exponential function, the lifetime is then determined by $\tau_m = \int t\varphi(t) \Big/ \int \varphi(t)$, where $\varphi(t)$ is the decay as a function of time *t*. The mean lifetime decreases from 55.5, 49.1, to 47.8 μs after the presence of Er^{3+} and further increase from 0.05 to 0.10 mol%. This can be attributed to the cross relaxation [Pr^{3+}($^1D_2$), Er^{3+}($^4I_{15/2}$)]→[Pr^{3+}($^1G_4$), Er^{3+}($^4I_{13/2}$)], by which some of the energy in Pr^{3+}:$^1D_2$ were transferred to neighboring Er^{3+} in the ground state due to the broad spectral overlap between them [see inset of Fig. 3(a)], resulting in a depleting of the Pr^{3+}:$^1D_2$. Another possible ET from Pr^{3+}:$^1D_2$ to Er^{3+}:$^4F_{9/2}$ can be ignored considering the large energy gap between them (~1490 cm^{-1}) and the relatively low phonon energy of the host (the maximum phonon energy is ~770 cm^{-1} according to the Raman spectrum). Indeed no emission from relevant Er^{3+} levels such as $^4F_{9/2}$ is observed in the Pr^{3+}-Er^{3+} codoped sample when excited at 594 nm (into the Pr^{3+}:$^1D_2$ absorption band). The overall efficiency can be evaluated by the quantum efficiency η_{QE} of the emitting level Pr^{3+}:$^1D_2$ which is calculated by $\eta_{QE} = \tau_m/\tau_r$, where τ_r is the radiative lifetime obtained by the Judd-Ofelt calculation [14]. The value of η_{QE}, which is 44.0% in the (0.3 mol%)Pr^{3+}-singly doped sample, shows a slight decrease after the codoping of Er^{3+} but remains above 38.0% in the (0.3 mol%)Pr^{3+}-(0.1 mol%)Er^{3+} codoped sample.

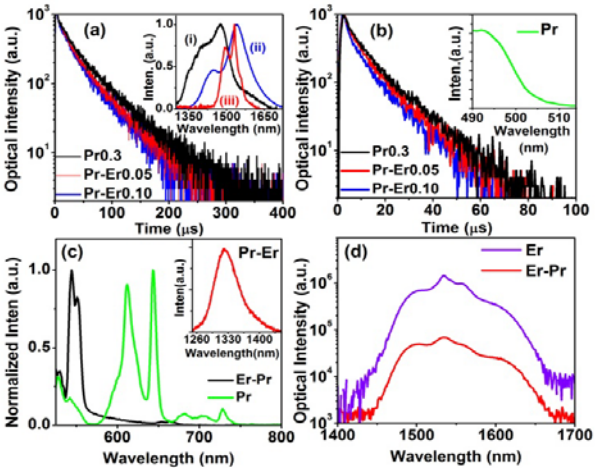

Fig. 3. Decay curves monitored at (a) 1420 nm and (b) 495 nm under 488 nm excitation. Inset of (a) shows the spectral overlaps between normalized (i) Pr^{3+}: $^1D_2$→$^1G_4$ emission band, (ii) Pr^{3+}: $^3F_{4,3}$←$^3H_4$ and (iii) Er^{3+}: $^4I_{13/2}$←$^4I_{15/2}$ absorption bands. Inset of (b) shows the Pr^{3+}: $^3P_0$→$^3H_4$ emission band under 488 nm excitation. (c) Visible emissions of Pr^{3+}-Er^{3+} codoped sample under 525 nm excitation and Pr^{3+}-doped sample under 488 nm excitation. Inset of (c) shows the Pr^{3+} 1.3 μm emission from Pr^{3+}-Er^{3+} codoped sample under 980 nm excitation. (d) Er^{3+} 1.53 μm emissions from Er^{3+}-singly doped and Pr^{3+}-Er^{3+} codoped samples under 980 nm excitation.

To further understand the phenomena observed, it is necessary to consider other energy transfer (ET) processes involved between Pr^{3+} and Er^{3+}. To investigate the ET process from Pr^{3+}:$^3P_0$ to Er^{3+}:$^4F_{7/2}$, we measured the Pr^{3+}: $^3P_0$→$^3H_4$ emission as well as its decay curves at monitoring wavelength of 495 nm under 488 nm excitation, and they are shown in Fig. 3(b) and inset. The lifetime shows a decrease for the Pr^{3+}-doped samples after the addition of Er^{3+}. This is in accordance with the decrease of 526, 611, and 643 nm emissions which originate from the common level Pr^{3+}:$^3P_0$, confirming the occurrence of the ET process Pr^{3+}($^3P_0$)→ Er^{3+}($^4F_{7/2}$). The ET from Er^{3+}:$^4S_{3/2}$ to Pr^{3+}:$^1D_2$ can be taken no consideration because the energy mismatch between them is as large as ~1580 cm^{-1}. This is also confirmed by the emission spectrum measured under excitation of 525 nm [see Fig. 3(c)] at which the excitation energy is absorbed only by Er^{3+}($^2H_{11/2}$). In Fig. 3(c), the Er^{3+} green emissions from Er^{3+}: ($^2H_{11/2}$,$^4S_{11/2}$)→$^4I_{15/2}$ transition are clearly observed while no Pr^{3+} relevant emission is

#159575 - $15.00 USD Received 9 Dec 2011; revised 23 Mar 2012; accepted 29 Mar 2012; published 14 May 2012

observed. The Er^{3+}:$^4I_{11/2}$ and Pr^{3+}:$^1G_4$ are quasi-resonant levels, and the ET process $Er^{3+}(^4I_{11/2})\rightarrow Pr^{3+}(^1G_4)$ occurred, which is confirmed by the observation of the Pr^{3+} 1.3 μm emission in Pr^{3+}-Er^{3+} codoped sample under 980 nm excitation, while there is no 1.3 μm emission observed in Pr^{3+}-singly doped sample under the same excitation. This ET was also observed in Er^{3+}-Pr^{3+} codoped ZBLAN glasses [24,25], and the 1.3 μm emission/amplification was obtained in Pr^{3+}-Yb^{3+} codoped fiber using a 980 nm laser diode pump [26]. As for the ET from the resonant levels of Er^{3+}:$^4I_{13/2}$ to Pr^{3+}:$^3F_{4,3}$, it is confirmed by the significant decrease of the Er^{3+} 1.53 μm emission after the addition of Pr^{3+}, as shown in Fig. 3(d). By depleting the terminal level of Er^{3+}: $^4I_{11/2}\rightarrow{}^4I_{13/2}$ transition through this resonant ET process, enhanced gain at 2.7-2.8 μm range was obtained in Er^{3+}-Pr^{3+} codoped ZBLAN fiber [27]. The relative increase of the Er^{3+} 1.23 μm emission compared with of 1.53 μm [see Fig. 2] can be ascribed to the improved population inversion between the upper and lower levels besides the decrease of 1.53 μm emission itself due to the ET3 process. Under 488 nm excitation, the emitting level Er^{3+}:$^4S_{3/2}$ is populated via the multi-phonon relaxations from Er^{3+}:$^4F_{7/2}$ followed the ET1 process and meanwhile the terminal level depleted by the ET from it to Pr^{3+}:$^1G_4$. The both contribute to an increase of the population inversion and thereafter the relatively enhanced 1.23 μm emission. All the ET processes involved are schematically illustrated in Fig. 4.

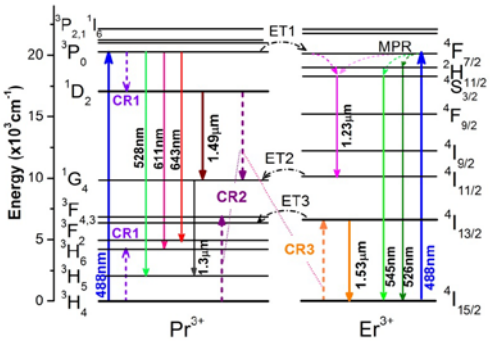

Fig. 4. Schematic energy-level diagram of Pr^{3+} and Er^{3+}, and possible energy transfer routes involved. ETi (i = 1,2,3), CRi (i = 1,2,3), and MPR represent energy transfer, cross relaxation, and multi-phonon relaxation processes, respectively.

The stimulated emission cross-section σ_{em} for the Pr^{3+}: $^1D_2\rightarrow{}^1G_4$ transition was determined to be 0.90×10^{-20} cm^2 by scaling the emission spectrum through the Füchtbauer-Ladenburg approach [28] because this transition occurs between the two excited states. Theσ_{em} of Pr^{3+} emission in fluorotellurite is larger than in bismuth gallate glass (0.70×10^{-20} cm^2) [16] and of Ni^{2+} in glass-ceramics (0.63×10^{-20} cm^2) [8], although smaller than the active Bi ions in germanate glass (1.59×10^{-20} cm^2) [4]. The σ_{em} for the Er^{3+}: $^4I_{13/2}\rightarrow{}^4I_{15/2}$ transition was derived to be 1.06×10^{-20} cm^2 using the McCumber relationship [29]. It is larger than those in TeZnNa (0.85×10^{-20} cm^2) [30] as well as many other types of oxides such as germanate (0.58×10^{-20} cm^2), silicate (0.73×10^{-20} cm^2), and phosphate (0.76×10^{-20} cm^2) [29].

4. Conclusions

Superbroadband near-infrared emission covering the expanded low-loss telecommunication window was achieved in Pr^{3+}-Er^{3+} codoped fluorotellurite glasses under 488 nm excitation. Er^{3+} is demonstrated to be a good candidate to compensate the quenching of Pr^{3+} near-infrared emission resulted from the cross relaxation process [$^1D_2$, $^3H_4$]→[$^1G_4$, $^3F_{3,4}$]. The results confirm that Pr^{3+}-Er^{3+} codoped fluorotellurite glass is promising for the superbroadband amplified spontaneous emission sources, optical amplification, and tunable lasers applications. Further investigations and experiments are underway.

#159575 - $15.00 USD Received 9 Dec 2011; revised 23 Mar 2012; accepted 29 Mar 2012; published 14 May 2012

Acknowledgments

The authors thank support from The Hong Kong Polytechnic University (grants G-YH91, G-YJ20, and A-PK72) and from the RGC of Hong Kong SAR, China (project CityU 119708).

#159575 - $15.00 USD Received 9 Dec 2011; revised 23 Mar 2012; accepted 29 Mar 2012; published 14 May 2012